

# Ferrofluid-based magnetorheological fluids: tuning the properties by varying the composition at two hierarchical levels

Daniela Susan-Resiga<sup>1,2</sup> · Ladislau Vékás<sup>3</sup>

Received: 29 November 2015 / Revised: 10 March 2016 / Accepted: 14 March 2016 / Published online: 29 March 2016  
© Springer-Verlag Berlin Heidelberg 2016

**Abstract** The magnetorheological behavior of three sets of ferrofluid-based magnetorheological (MR) fluids is investigated to determine the dependence of the static and dynamic yield stresses, as well as of the magnetoviscous effect on the volume fraction of magnetite nanoparticles  $\varphi$  and of the added Fe particles  $\Phi_{Fe}$ , at different values of the magnetic induction  $B$  in the MR cell. A wide range of the magnetic particle volume fractions were considered at the two hierarchical levels involved: at the nanometer level,  $\varphi = 2.75, 11.67,$  and  $22.90 \%$ , and at the micrometer level,  $\Phi_{Fe} = 5\text{--}40 \%$ . Taking into account also the oleic acid monolayer coating of the magnetite nanoparticles, the hydrodynamic volume fraction of the most concentrated ferrofluid results to be  $65 \%$  and, consequently, the highest value of the effective total volume fraction of the investigated extremely bidisperse MR fluids attains  $85 \%$ . The diagrams of the static and dynamic (Bingham) yield stresses and of the magnetoviscous effect offer an adequate choice of the nanometer and micrometer range particle volume fractions to fulfill the specific requirements of high-pressure rotating seals and of various MR devices.

**Keywords** Ferrofluid · Magnetorheological fluid · Nano-micro composite fluid · Yield stress · Magnetoviscous effect · MR effect

## Introduction

Magnetorheological (MR) fluids are the basic components of many high-tech devices devoted to the control of vibrations or transmission of torque (Carlson and Jolly 2000, Klingenberg 2001), sometimes in severe exploitation conditions (Barber 2013). MR control devices for use in real-world civil engineering applications (Friedman and Dyke 2013) imply even more expectations concerning long-term operating capabilities of MR fluids. The need to improve the performances of MR devices motivates the increasing interest for new MR formulations (Bossis et al. 2002; Lopez-Lopez et al. 2005; Wereley et al. 2006; Park et al. 2010; de Vicente et al. 2011; Liu and Choi 2012; Liu et al. 2012; Shah et al. 2014) adapted to specific requirements deriving from constructive and functional details of MR fluid damper systems (Wang and Gordaninejad 2006; Zhu et al. 2012, Iglesias et al. 2014).

Colloidal magnetic nanoparticles of several tens of nanometers used as additives (Wereley et al. 2006) or of less than 10 nm in ferrofluids used as carriers (Lopez-Lopez et al. 2005) proved to be an efficient way to improve the kinetic stability and magnetic-field-induced yield stress of MR fluids. Among the new MR formulations analyzed in de Vicente et al. (2011), the ferrofluid-based suspensions of micrometer-size iron particles (López-López et al. 2006, Yang et al. 2009, Susan-Resiga et al. 2010, Iglesias et al. 2012) are very promising in exploiting the advantages both of ferrofluids and conventional MR fluids (Vekas 2008). Such two very different hierarchical levels (several nanometers and a few micrometers) proper to ferrofluid-based MR fluids give a larger field-induced yield stress (Wang

---

✉ Ladislau Vékás  
vekas.ladislau@gmail.com; vekas@acad-tim.tm.edu.ro

<sup>1</sup> Research Center for Engineering of Systems with Complex Fluids, University Politehnica Timisoara, Timisoara, Romania

<sup>2</sup> Faculty of Physics, West University of Timisoara, Timisoara, Romania

<sup>3</sup> Laboratory of Magnetic Fluids, Center for Fundamental and Advanced Technical Research, Romanian Academy-Timisoara Branch, Timisoara, Romania

and Gordaninejad 2006; de Vicente et al. 2011), due to the increased interaction between multidomain Fe particles, multiplied by the magnetic permeability of the ferrofluid carrier (Bossis et al. 2002). Also, due to the fact that the magnetic nanoparticles are permanent magnets distributed around each micron-size Fe particle, the surface-to-surface contact between Fe particles is prevented, improving redispersibility after sedimentation (López-López et al. 2005; Iglesias et al. 2012). Experimental tests of a monotube MR shock absorber (Iglesias et al. 2014) show that the use of ferrofluid-based MR fluid represents a suitable alternative to conventional MR fluids involving various additives (surfactants, thickening polymers, silica nanoparticles, etc.) to prevent aggregation and irreversible sedimentation of the micrometer-size Fe particles. Comparative investigations show larger friction coefficient and considerably reduced wear in case of ferrofluid-based than conventional MR fluids (Iglesias et al. 2015), attributed to the protective “halo” of surfacted magnetite nanoparticles around the iron microparticles of the MRF. Avoiding wear is particularly important for long-term operating rotating seal applications. Referring to the colloidal stability of the ferrofluid carrier, the agglomerate formation at the nanolevel could have significant influence on the overall MR behavior of the nano–micro composite MR fluid. Ferrofluids with clustered iron oxide nanoparticles show slow relaxation of the shear stress in magnetic field after a stepwise change of the shear rate (Borin et al. 2014). The time of the transient can reach several minutes due to the process of structure formation and destruction under the simultaneous action of the applied magnetic field and shear flow, which could influence in a hardly controllable way the short time, within 1–2-ms MR response of a ferrofluid-based magnetorheological suspension. In this respect, the colloidal stability of the ferrofluid carrier, achieved by electrostatic or steric stabilization of magnetic nanoparticles in water or organic carrier respectively, is of utmost importance to avoid field-induced cluster formation or even gas–liquid-type phase transition, observed especially in ionic ferrofluids (Cabuil et al. 1996) proposed also as carrier for water-based composite MR fluids (Viota et al. 2007; Viota et al. 2009).

The present study was motivated by the increasing interest for MR fluids with reduced wear and improved sedimentation–redispersion behavior to be used in various MR devices, as mentioned above. Among others, ferrofluid-based iron particle suspensions are envisaged for high-pressure rotating magnetofluidic seals (Borbath et al. 2011), MR brake designed to control the rotating speed of hydraulic runners (Bosioc et al. 2014), and a new type of seismic MR damper, all under development in our laboratory and requiring very different magnetic and flow characteristics. For example, rotating seal applications (Fujita et al. 1999) are limited with conventional MR fluids, as under static conditions the micron-size Fe particles rapidly separate from the non-magnetic carrier in the strongly non-uniform magnetic field

of a sealing stage. This separation in field gradient does not take place for concentrated ferrofluid-based MR fluid (Borbath et al. 2014), but a compromise has to be found between the saturation magnetization (as high as possible to achieve high sealing capacity) and an acceptable level of the magnetoviscous effect, depending on the fluid composition and the operating conditions of the rotating seal. By means of controlling the particle concentration at both hierarchical levels, the magnetorheological properties of the resulting MR fluids can be tailored to offer a lubricant with improved field-controlled response for semi-active dampers and brakes, as well as for rotating seals.

In a previous paper (Susan-Resiga and Vekas 2014), we have shown that the addition of micrometer-sized iron particles to a concentrated ferrofluid without any supplementary stabilizing agent is a direct and simple way to control the yield stress and magnetoviscous behavior, as well as the saturation magnetization of the resulting nano–micro composite fluid. In this paper, we investigate the magnetorheological behavior of three sets of ferrofluid-based MR fluids varying the volume fraction of both the nanometer-range magnetite nanoparticles and the micron-size Fe particles in order to evidence a wide range of possible choices of the adequate composition to fulfill the requirements of various MR devices. The scope is to determine the dependence of the static and dynamic yield stress, as well as of the magnetoviscous effect on the volume fraction of magnetite nanoparticles and of the added Fe particles, at different values of the magnetic induction in the MR cell. We used as carrier practically agglomerate-free, high colloidal stability ferrofluids with Newtonian behavior in the absence of a magnetic field. This is essential to keep the off-state viscosity of the nano–micro composite fluids as low as possible and to prevent formation of irreversible agglomerates, which could increase the zero field viscosity and affect the reproducibility of MR response of the composite fluid samples. Also, the possible wall slip effects were thoroughly investigated, previously not considered for ferrofluid-based magnetorheological fluids.

The relationships extracted by fitting the experimental data offer detailed correlation between nanolevel and microlevel composition and the MR response to meet the specific requirements of various MR devices and rotating seals.

## Experimental

### Preparation of samples

There were prepared three sets of samples, with each of them having nine extremely bidisperse composite fluids of micrometer-size Fe particles dispersed in transformer-oil-based ferrofluids with three different volume concentrations of magnetite nanoparticles,  $\phi = 2.75, 11.67, \text{ and } 22.90\%$ .

The high colloidal stability ferrofluids were obtained at the Research Center for Engineering of Systems with Complex Fluids, University Politehnica Timisoara, by chemical coprecipitation and sterical stabilization procedure, as described in Bica et al. (2000) and Vékás et al. (2007). This type of ferrofluid for rotating seal applications, with chemisorbed oleic acid monolayer coated magnetite nanoparticles of 6.9 nm and no excess surfactant, shows very reduced particle clustering and Newtonian flow behavior (Susan-Resiga et al. 2012). The preexisting particle aggregates trapping also an amount of carrier liquid would reduce the achievable maximum packing fraction (Russel et al. 1989; Zhou et al. 1995). The Fe particles (product of Merck KGaA, code 1.03819.0500) are multidomain ferromagnetic particles with 10- $\mu\text{m}$  mean size.

The volume fraction values of iron powder  $\Phi_{Fe}$  dispersed in the ferrofluid carriers are given in Table 1. The iron powder was

dispersed by prolonged mechanical stirring of the Fe particle–ferrofluid mixture, without addition of any surfactant. Special care was taken to eliminate the air bubbles from the nano–micro composite fluid before measurement. The total volume fraction of particles in a sample is given by the relationship  $\Phi_{tot} = \Phi_{Fe}(1 - \phi) + \phi$  (Susan-Resiga and Vékás 2014), where  $\phi$  represents the volume fraction of magnetite nanoparticles. The saturation magnetization of the most concentrated (volume fraction 22.90 %) ferrofluid carrier is 930 G. By adding Fe particles, the magnetization increases linearly up to 10,772 G for 56.82 % total particle volume fraction. The rheological behavior of these bidisperse samples was compared with that of a commercial magnetorheological fluid sample (MRF 140 CG, product of Lord Co., USA), having micrometer-sized Fe particles ( $\Phi_{Fe} = \Phi_{tot} = 40\%$ ) in a hydrocarbon carrier.

### Magnetorheological characterization

The measurements were performed using a PHYSICA MCR 300 rheometer (Anton Paar) with magnetorheological cell (MRD /TI-SN18581). The MR cell has parallel plates of 20-mm diameter, with the gap being fixed at  $h = 0.2$  mm. All the tests were done at 20 °C. The magnetic flux density was determined using a Hall probe located as described in Laun et al. (2008, 2010) to ensure on-line measurement of the magnetic induction in the MR cell gap.

In order to ensure as much as possible the homogeneity of a sample supposed to MR tests, the experimental procedure consists in intense mixing of the nano–micro composite fluid just before to fill it into the MR cell, followed by a preshearing of 30 s at  $\gamma = 100\text{ s}^{-1}$  and by application for 15 s of a magnetic field corresponding to the planned test. The MR test was performed after a waiting period of 120 s.

It is worth to mention the issues related to precise delivery of the required amount of sample into the gap of the MR cell. Taking into account the gap size,  $h = 0.2$  mm, and the diameter of the parallel plates,  $2R = 20$  mm, the required volume of sample is very small,  $V = 0.063$  ml, and consequently the exact sampling becomes difficult especially for the most concentrated ferrofluid-based MR fluids (the set F 1000). This explains the somewhat greater dispersion of the experimental points in this case.

## Results and discussion

### Flow curves in magnetic field

The viscosity curves for the three ferrofluid carriers, F 100, F 500, and F 1000, are given in Fig. 1 for various values of the magnetic induction  $B$  measured in the MR cell. In zero field, the curves show Newtonian behavior for all the three ferrofluids. The Newtonian behavior of the sample F 1000,

**Table 1** Nano–micro composite MRF samples

Sample	Iron particle volume fraction $\Phi_{Fe}$ (%)	Total volume fraction $\Phi_{tot}$ (%)
F 100	0	2.75
F 100–1	5	7.33
F 100–2	10	12.21
F 100–3	15	17.08
F 100–4	20	21.96
F 100–5	25	26.84
F 100–6	30	31.72
F 100–7	35	36.59
F 100–8	40	41.47
F 500	0	11.67
F 500–1	5	16.09
F 500–2	10	20.50
F 500–3	15	24.92
F 500–4	20	29.34
F 500–5	25	33.75
F 500–6	30	38.17
F 500–7	35	42.59
F 500–8	40	47
F 1000	0	22.90
F 1000–1	4	25.98
F 1000–2	10	30.61
F 1000–3	15	34.47
F 1000–4	20	38.82
F 1000–5	25	42.18
F 1000–6	30	46.03
F 1000–7	35	47.96
F 1000–8	44	56.82
MRF 140 CG	40	40

F 100, F 500, and F 1000 denote the ferrofluid (nanofluid) carriers having 100, 500, and 1000 G nominal saturation magnetization

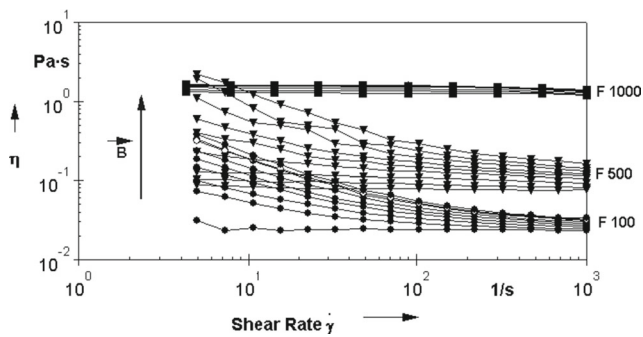


**Fig. 1** The viscosity curves for the three ferrofluid carriers, F 100, F 500, and F 1000, for different values of the magnetic induction  $B$  corresponding to electrical current values  $I = 0, 0.1, 0.25, 0.5, 0.75, 1, 1.5, 2,$  and  $3$  A in the coil of the MR cell

with the volume fraction of the magnetic nanoparticles  $\phi = 22.90\%$ , denotes that particle agglomerates are practically absent up to the highest concentration of particles and evidences the efficiency of the steric stabilization applied. In non-zero field, due to field-induced temporary agglomerates, the samples show magnetoviscous effect especially for reduced shear rate values. The field-induced temporary agglomerates are progressively destroyed at increasing shear rates, as evidenced by the decreasing values of the viscosity at high shear rates (Fig. 1).

Following the dispersion of micrometer-size Fe particles in the ferrofluid carriers, the flow behavior changes significantly and the suspensions become shear thinning as a consequence of the competitive actions of the magnetic field and shearing giving rise to agglomerate formation and fragmentation processes (de Vicente et al. 2011) and to a much more pronounced magnetoviscous effect than in case of the ferrofluid carriers F 100, F 500, and F 1000. This is exemplified in Fig. 2a where the viscosity curves of the most concentrated ferrofluid F 1000 ( $\Phi_{Fe} = 0\%$ ) and of the composite fluid F 1000–4 ( $\Phi_{Fe} = 20\%$ ) are presented comparatively. This type of viscous behavior is observed also for the other ferrofluid-based Fe particle suspensions. The magnetic nanoparticle content at the same total solid particle volume fraction has a significant effect on the viscous behavior in the absence and in the presence of the magnetic field. This is illustrated by the viscosity curves resulted by varying the composition at both hierarchical levels keeping the total particle volume fraction at a certain value, such as approximately 26 % (Fig. 2b). While the solid content is the same, the flow behavior is very different depending on the composition details.

To verify if wall slipping effects influence the measurements, the flow and viscosity curves were measured repeatedly (five times) under identical conditions as indicated in (Mezger 2002, p.32). The reproducibility of data was examined for measurements in the absence of the field and for the

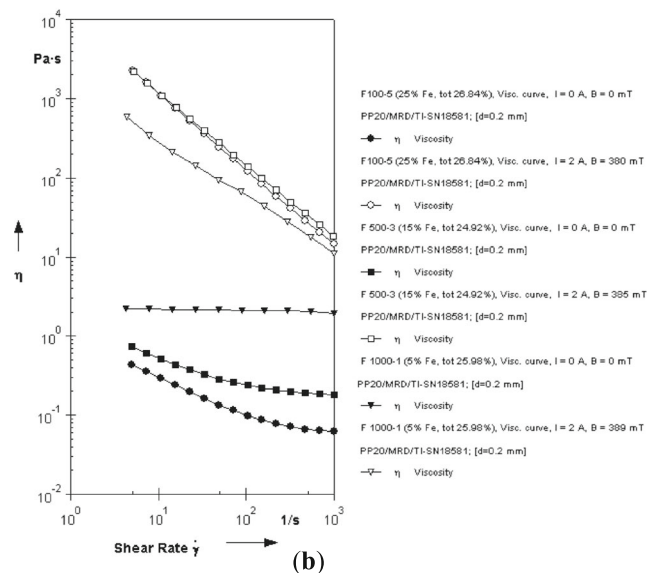
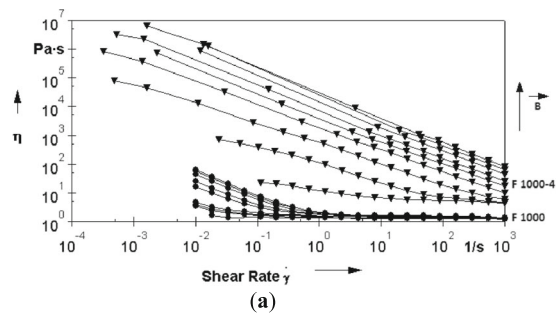


**Fig. 2** Viscosity curves in the absence and in the presence of the applied magnetic field **a** for the most concentrated ferrofluid F 1000 ( $\Phi_{Fe} = 0\%$ ) and of the composite fluid F 1000–4 ( $\Phi_{Fe} = 20\%$ ); the values of the magnetic induction correspond to electrical current values  $I = 0, 0.1, 0.25, 0.5, 0.75, 1, 1.5, 2,$  and  $2.5$  A in the coil of the MR cell and **b** for three samples with increasing magnetic nanoparticle volume fraction, for  $I = 0$  A and  $I = 2$  A

highest applied magnetic field for the samples F 500–4 and MRF 140 CG (Fig. 3a, b). Perfect superposition of the experimental points is observed for  $h = 0.2$  mm between the parallel plates of the MR cell. The tests were repeated (also five times), according to Yoshimura and Prud'homme (1988) and Durairaj et al. (2010) also for a larger gap value  $h = 0.4$  mm. Again, it is observed the superposition of flow and viscosity curves with those for  $h = 0.2$  mm, both for zero and non-zero applied field (Fig. 3a, b), which demonstrates the absence of any wall slip effect.

### Dynamic yield stress

The dynamic yield stress, defined as the minimum shear stress needed to maintain the flow of the material after the breaking of the thixotropic structure, gives a quantitative measure of the point corresponding to the breaking of all the structures

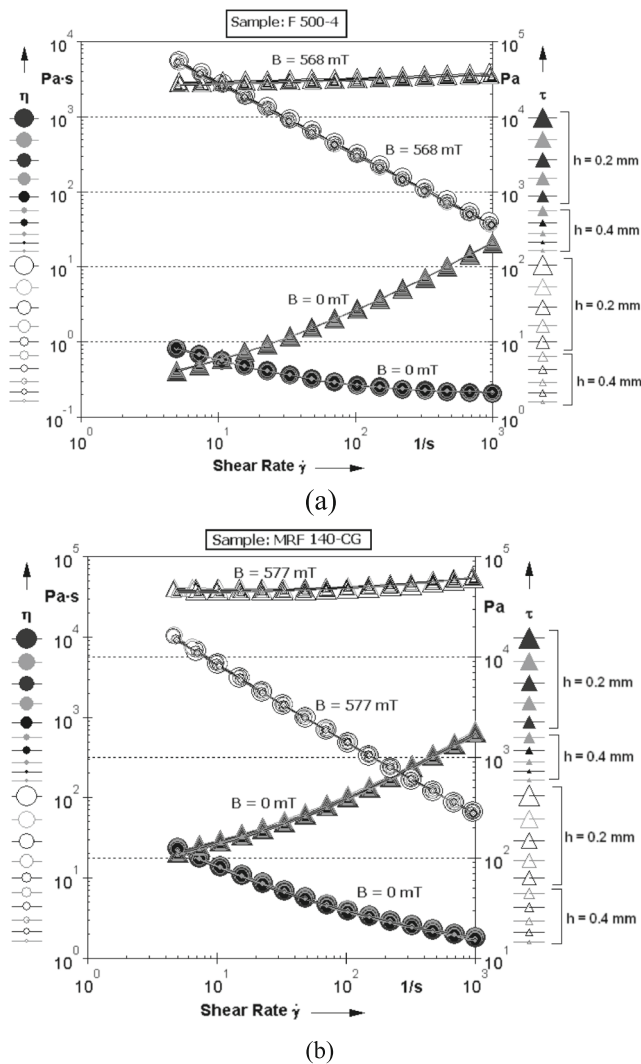
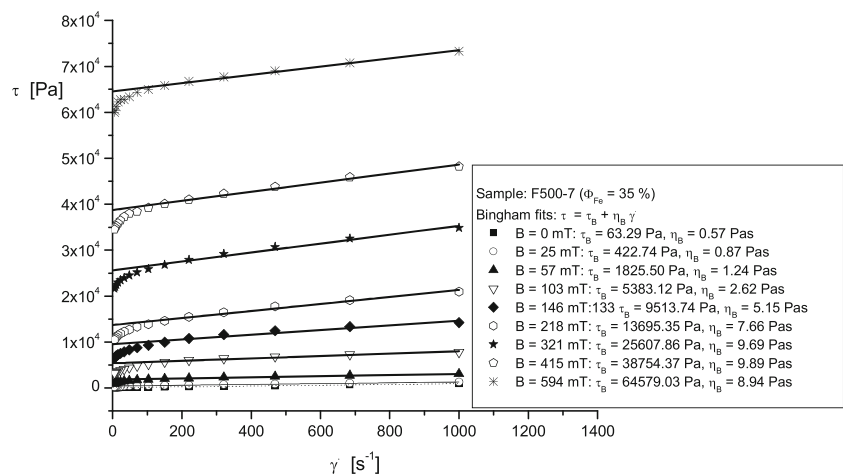


**Fig. 3** Reproducibility tests of measurements for two values of the MR cell gap ( $h = 0.2$  mm and  $h = 0.4$  mm) and for  $B = 0$  mT and  $B = 568$  (577) mT: **a** sample F 500–4; **b** sample MRF 140 CG

formed in the suspension, when the flow becomes Newtonian (López-López et al. 2006).

**Fig. 4** Determination of the dynamical yield stress by fitting the flow curves to the Bingham model, for all the measured magnetic induction values ( $B$ )—sample F 500–7 ( $\Phi_{Fe} = 35\%$ ). The fits do not consider the shear stress values at low shear rates



To determine the dynamic yield stress of each sample, the flow curves were fitted using the Bingham model (e.g., Fig. 4):

$$\tau = \tau_B + \eta_B \gamma \tag{1}$$

where the fit parameters are the following:

$\tau_B$  = the dynamic yield stress (according to the Bingham model)

$\eta_B$  = the Bingham viscosity

The dependences of the static and dynamic yield stresses on the particle volume fraction and the magnetic induction are of great significance for engineering applications (Klingenberg et al. 2007, de Vicente et al. 2011, Susan-Resiga and Vékás 2014). In Fig. 5a–c, the dependencies of the dynamical yield stress on the magnetic induction for the three sets of samples given in Table 1, determined by fitting the flow curves with the Bingham model, except the low shear rate domain are represented. For comparison, the diagrams contain also the data corresponding to a commercial MR fluid (MRF 140 CG, LORD Co.) having 40 % volume fraction of Fe particles dispersed in a hydrocarbon carrier.

The diagrams in Fig. 5 evidence the strong MR effect for all the three sets of samples. The Bingham yield stress  $\tau_B$  increases with both the magnetite nanoparticle (NP) volume fraction  $\phi$  and the Fe particle volume fraction  $\Phi_{Fe}$  and, consequently, with the total particle volume fraction  $\Phi_{tot}$ . For the set of samples F 1000, a weak saturation tendency of the MR effect is observed in Fig. 5c, which may be attributed to the high zero field viscosity and close packing of nanoparticles (hydrodynamic volume fraction 65 %; the “The influence of particle volume fraction on the yield stress” section) leaving no place for temporary field-induced agglomerates of nanoparticles and any significant viscosity increase of the F 1000 carrier (Fig. 1). The high relative permeability of the carrier increases the interaction between the large Fe particles and favors the formation of agglomerates already at intermediate

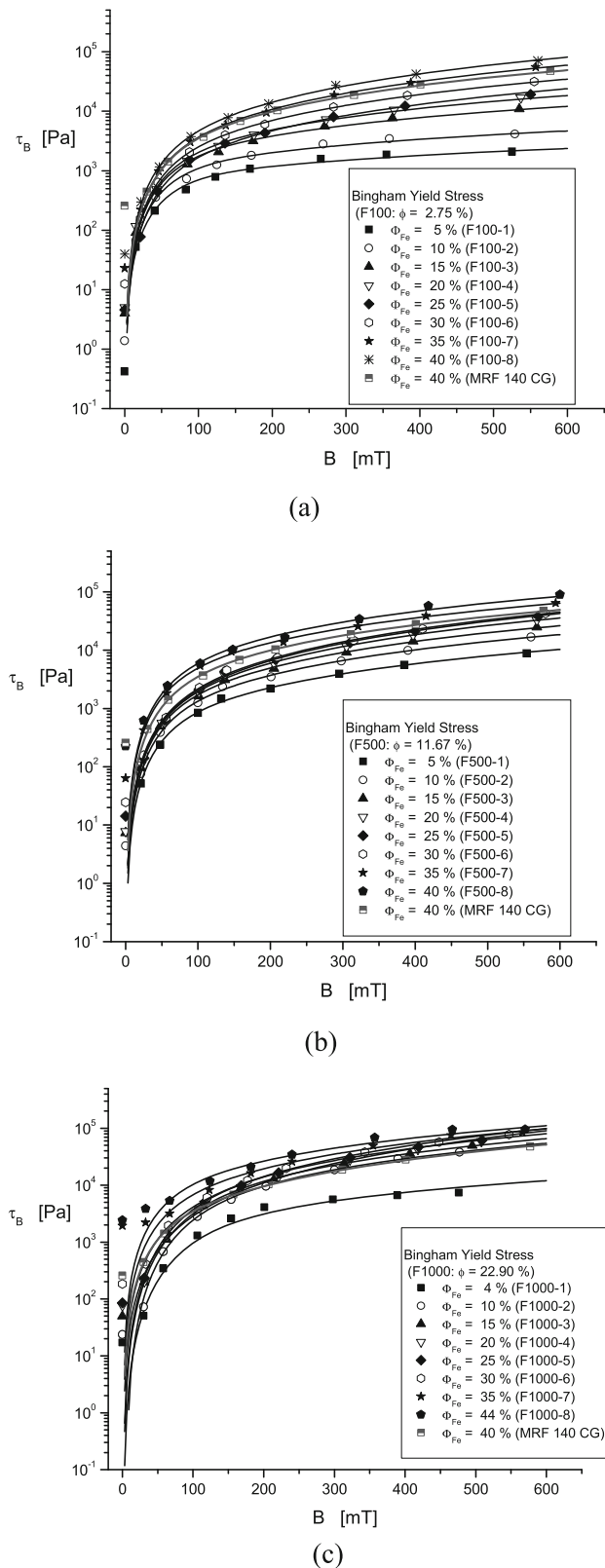


**Fig. 5** Dependence of the dynamic (Bingham) yield stress on the magnetic induction  $B$ ; the fits for the commercial MRF 140 CG and for the nano-micro composite samples: **a** set F 100, **b** set F 500, and **c** set F 1000

values of the applied magnetic field. Details of the composition of ferrofluid (FF)-based MR fluids giving enhanced MR response in comparison with the commercial sample will be discussed related to the yield stress diagrams in Figs. 7, 8, and 9.

### Fits of the magnetic field dependence of yield stress

For a quantitative description of the magnetic field dependence of the static and dynamic yield stresses (Fig. 5), the experimental data were correlated with the following formula that we proposed and used before in Susan-Resiga and Vékás (2014):

$$\tau_B = c_1 \left( \frac{B}{B^*} \right)^2 \left[ 1 - \tanh \left( \frac{B}{B^*} \right) \right] + c_2 \Phi_{tot}^n \left( \frac{B}{B^*} \right)^m \tanh \left( \frac{B}{B^*} \right) \quad (2)$$

The function  $\tanh x$ , which vanishes for  $x \rightarrow 0$  and is approaching 1 for  $x \rightarrow \infty$ , will be used “to connect” the two models describing the magnetic field dependence of the yield stress, as follows:

- The  $B^2$ -type dependence for small values of  $B$  (de Vicente et al. 2011; Park et al. 2010; Ramos et al. 2011; Yang et al. 2009)
- The sub-quadratic dependence for great values of  $B$ , where it is also a significant influence of the particle volume fraction (de Vicente et al. 2011, Ginder et al. 1996), described by the relationship  $\Phi_{tot} = \Phi_{Fe}(1 - \phi) + \phi$  (Susan-Resiga and Vékás 2014)

In relation (2),  $B^*$  represents the value of the magnetic induction at which the transition between the two kinds of behaviors occurs. The increase of field-induced particle structures becomes slower as the agglomerate size approaches the maximum in the given conditions (especially the composition details) and the yield stress versus magnetic induction curves change slope (Ramos et al. 2011). The fit parameters are  $c_1$ ,  $c_2$ ,  $n$ ,  $m$ , and  $B^*$ .

The procedure applied to fit the experimental data is presented below.

At first, the fit was applied only to the initial quadratic dependence of the yield stress using experimental data up to the value of the magnetic induction value corresponding to the transition, approximately at  $B^* = 100$  mT and the formula  $\tau_B = c_1 \left( \frac{B}{B^*} \right)^2$ , to obtain the value of  $c_1$ . Then, the whole sets of experimental data were used in the fits, keeping fixed the value already obtained for  $c_1$  and  $B^* = 100$  mT, with the remaining fit parameters being  $c_2$ ,  $n$ , and  $m$ .

For all the three sets of samples (and also for the MRF 140 CG commercial sample), the fit parameters  $c_1$ ,  $c_2$ , and  $m$

increase and  $n$  decreases for increasing values of  $\Phi_{Fe}$ , respective  $\phi$ , as follows:

$$c_1 = (696.73 \div 9720.47)Pa, c_2 = (1000.26 \div 3212.26)Pa, m = (0.68 \div 2.09), n = (0.14 \div -2.09)$$

**Static yield stress**

The static yield stress, defined as the shear stress value at which the material begins to flow, is related to the transition from solid to viscoplastic state. The static yield stress was determined applying the method given by Yang et al. (2009), using the *strain sweep mode* test. The static yield stress is represented by the maximum of the  $\tau = \tau(\gamma)$  curve when the sample is supposed to a logarithmic increase of the shear strain  $\gamma$  (see Fig. 6 for sample F 500–1). At great values of the particle volume fraction and of the deformation, the shear stress becomes increasingly unstable. These oscillations of the shear stress could be related to the rupture and rebuild of large chain-like agglomerates in concentrated samples under the influence of the applied field (Yang et al. 2009, Susan-Resiga and Vékás 2014).

The dependence of the static yield stress on the magnetic induction,  $\tau_y = \tau_y(B)$ , is outlined in Fig. 7a–c for the three sets of FF-based Fe particle suspensions; for comparison, the data for the commercial sample MRF 140 CG are also represented.

As it follows from Fig. 7, the static yield stress has a similar dependence on the magnetic induction  $B$  and on the  $\Phi_{Fe}$  as the dynamic yield stress. The highest values of the static yield stress were obtained for the most concentrated F 1000 set of samples. These values of the static yield stress are also higher than those measured

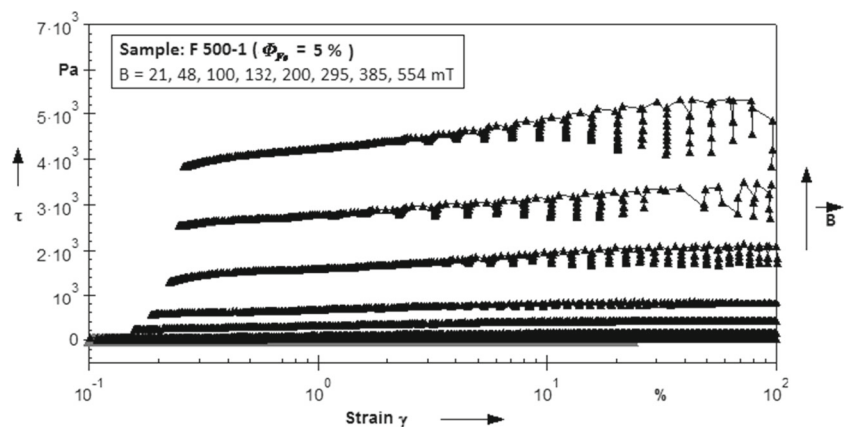
for the commercial sample (MRF 140 CG); e.g., for  $B > 200$  mT, the sample F 1000–2 ( $\Phi_{Fe} = 10\%$ ,  $\Phi_{tot} = 30.61\%$ ) shows greater static yield stress than the fluid MRF 140 CG ( $\Phi_{Fe} = \Phi_{tot} = 40\%$ ).

The correlation of  $\tau_y = \tau_y(B)$  data of Fig. 7 was performed using also a formula similar to (2), as in case of the  $\tau_B = \tau_B(B)$  dependence. As before, for all the three sets of samples (and also for the MRF 140 CG commercial sample), the fit parameters  $c_1$ ,  $c_2$ , and  $m$  increase and  $n$  decreases for increasing values of  $\Phi_{tot}$ , as follows:

$$c_1 = (93.47 \div 9955.12)Pa, c_2 = (182.51 \div 3275.11)Pa, m = (1.15 \div 2.41), n = (0.22 \div -2.02)$$

Beside the more intense MR effect, the ferrofluid-based multidomain Fe particle suspensions—extremely bidisperse MR fluids with nanometer-range magnetite nanoparticles and micrometer-size Fe particles—have also other advantages over the conventional MR fluids, with only Fe particles of several micrometer mean size. In the absence of applied field, the magnetic nanoparticles improve the sedimentation stability and redispersibility of the large Fe particles (de Vicente et al. 2011, López-López et al. 2005, Iglesias et al. 2012, Viota et al. 2009, Wereley et al. 2006, Yang et al. 2009, Ngatu and Wereley 2007); indeed, these are due to local alignment and network formation of the magnetic nanoparticles with permanent magnetic moment between the multidomain Fe particles (Bossis et al., 2002). Referring to the sedimentation–redispersion behavior of the three sets of ferrofluid-based MR fluids and the commercial MR fluid investigated in this work, the redispersion of F 100 samples and of the MRF 140 CG sample proved to be more difficult than in case of the F 500 and F 1000 sets with higher concentration of magnetite nanoparticles.

**Fig. 6** Results of the strain sweep mode test for the sample F 500–1, for all the values of the magnetic induction  $B$



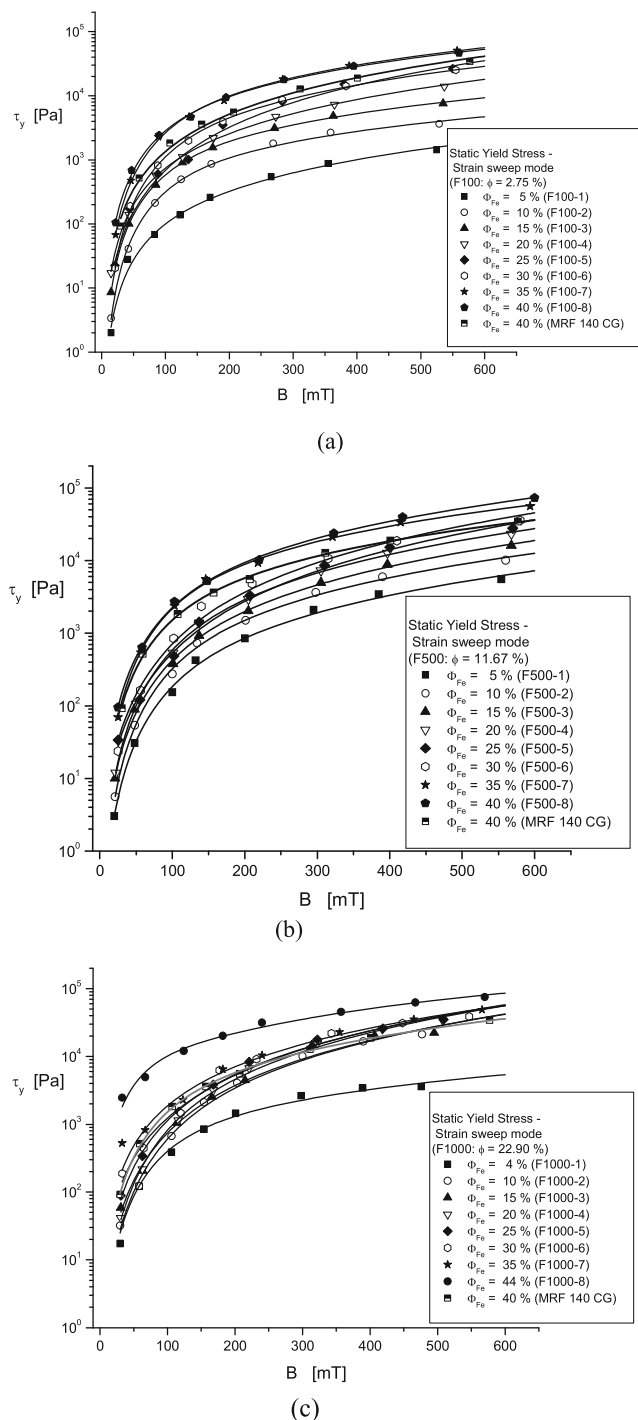


**Fig. 7** Dependence of the static yield stress on the magnetic induction B; the fits for the commercial MRF 140 CG and for the nano–micro composite fluid samples: **a** set F 100, **b** set F 500, and **c** set F 1000

**The influence of particle volume fraction on the yield stress**

The experimental curves of the magnetic field dependence of the dynamic (Bingham) and static yield stresses on the Fe particles volume fraction  $\Phi_{Fe}$  for different values of the magnetic nanoparticles volume fraction  $\phi$  are represented in

Figs. 8a–c and 9a–c for the ferrofluid-based MR fluids and also for the commercial sample MRF 140 CG.

The measured data represented in Figs. 8 and 9 illustrate the role of both the magnetic nanoparticle and the Fe particle

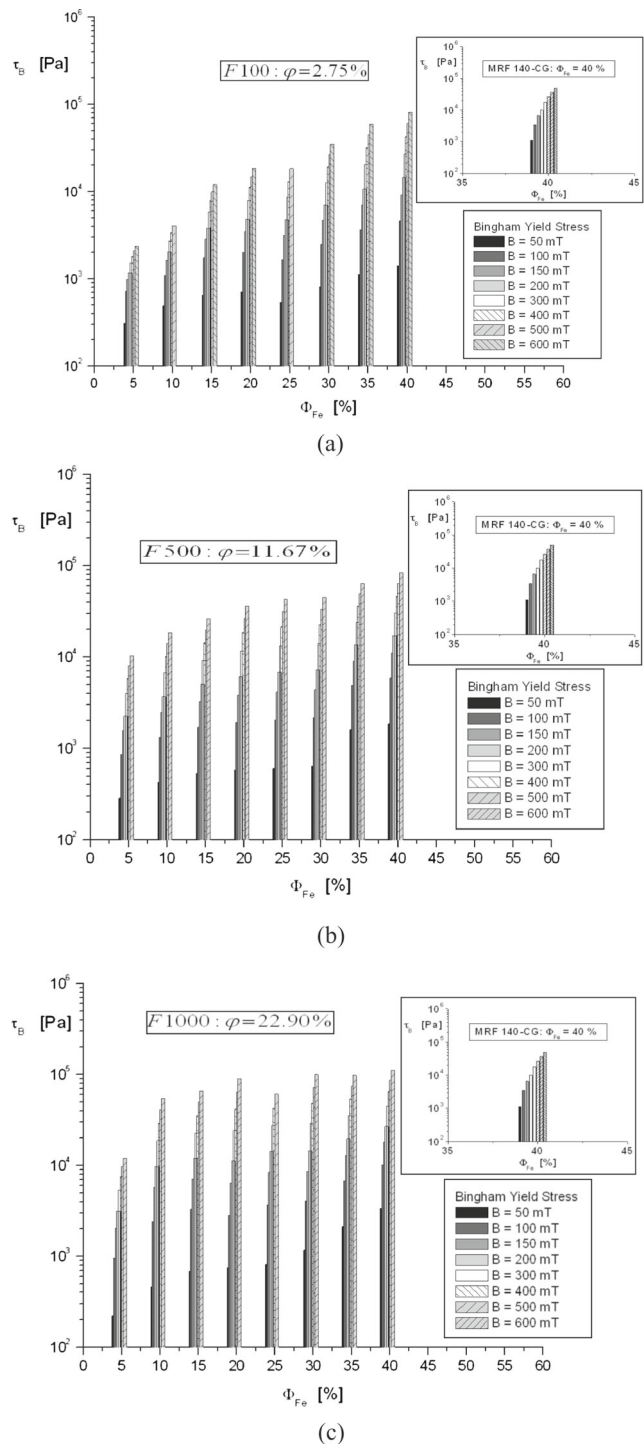


**Fig. 8** The dependence  $\tau_B = \tau_B(\Phi_{Fe})$  for different values of the magnetic induction B—MRF 140 CG in comparison with **a** the set F 100, **b** the set F 500, and **c** the set F 1000



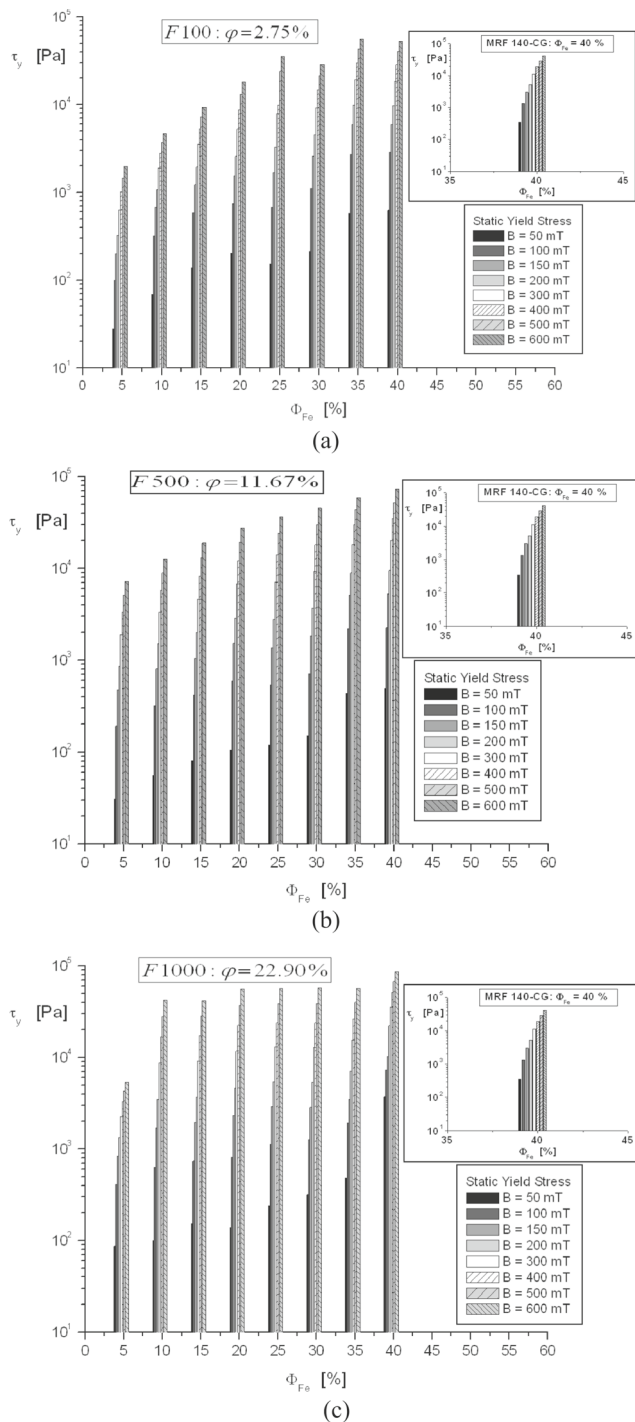


**Fig. 9** The dependence  $\tau_y = \tau_y(\Phi_{Fe})$  for different values of the magnetic induction  $B$ —MRF 140 CG in comparison with **a** the set F 100, **b** the set F 500, and **c** the set F 1000

volume fractions, evidenced by the composition details (volume concentration of magnetic nanoparticles (FF saturation magnetization) vs. volume fraction of micron sized particles). The curves clearly show the greater MR effect in case of ferrofluid-based MR fluids in comparison with conventional

MR fluids (sample MRF 140 CG), at the same particle volume fraction:

- Set F 100 ( $\phi = 2.75\%$ ):  $\tau_B$  and  $\tau_y$  are greater than the corresponding values for the commercial sample, starting with sample F 100–7 ( $\Phi_{Fe} = 35\%, \Phi_{tot} = 36.59\%$ ).
- Set F 500 ( $\phi = 11.67\%$ ):  $\tau_B$  values starting with sample F 500–7 ( $\Phi_{Fe} = 35\%, \Phi_{tot} = 42.59\%$ ) and  $\tau_y$  values starting with F 500–6 ( $\Phi_{Fe} = 30\%, \Phi_{tot} = 38.17\%$ ) are greater than those measured for the commercial sample.
- Set F 1000 ( $\phi = 22.90\%$ ):  $\tau_B$  and  $\tau_y$  are greater for samples starting with F 1000–4 ( $\Phi_{Fe} = 20\%, \Phi_{tot} = 38.82\%$ ) than the values determined for the commercial sample.

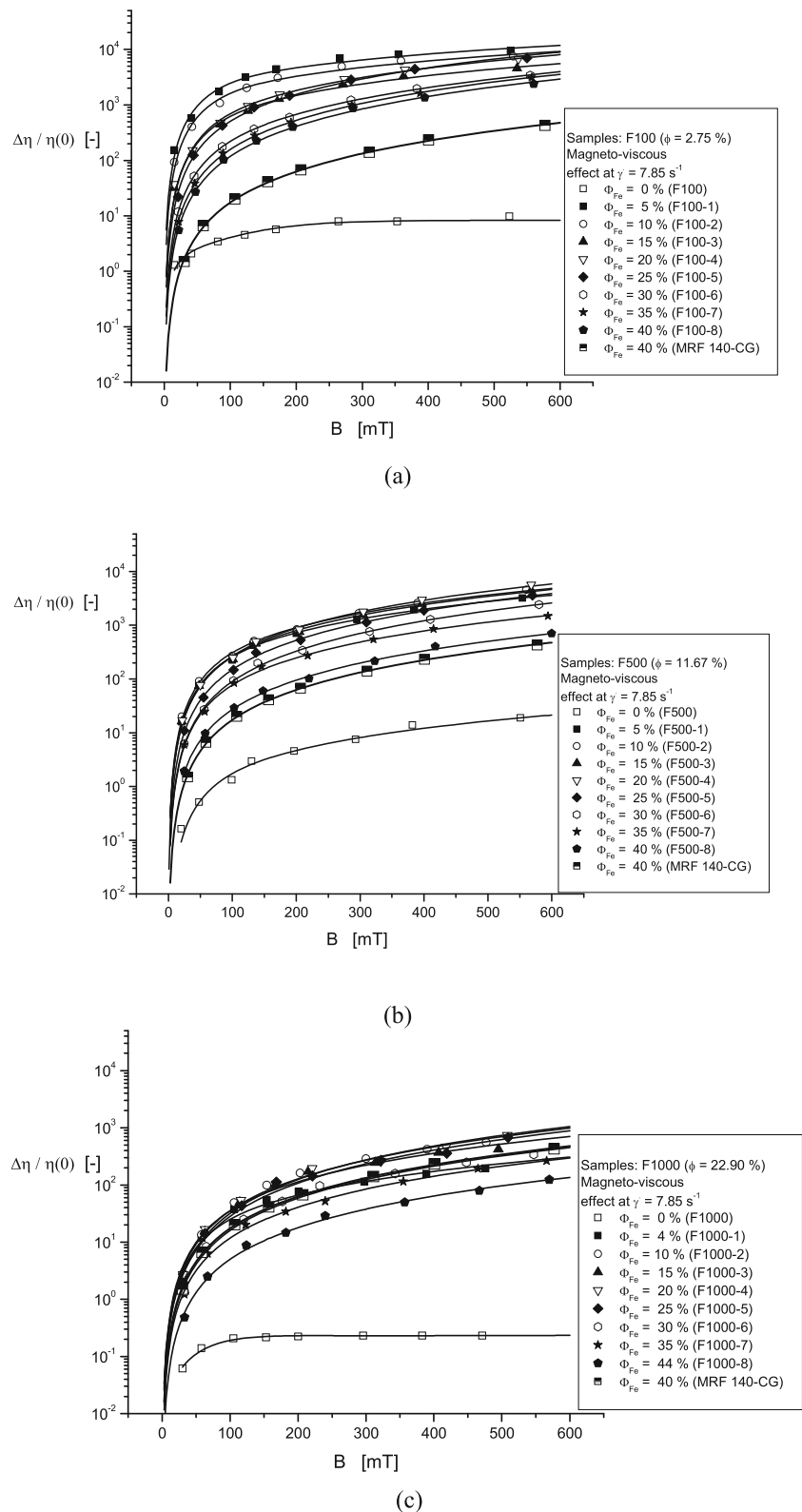
Also, for  $B > 200$  mT, the MR effect measured for the extremely bidisperse suspensions—ferrofluid-based MR fluids—is in general greater than that specific for the commercial sample, even for smaller particle volume fraction values.

The influence of composition details and particle volume fraction on the MR effect (de Vicente et al. 2011) is an essential feature to be considered for the design of high-performance MR devices (Zhu et al. 2012). The yield stress (dynamic and static) show an approximately linear increase for relatively small particle volume fraction values (up to 25%) (Rankin et al. 1999; de Vicente et al. 2011). For higher values, a non-linear, more rapid increase of the yield stress was observed (de Vicente et al. 2011, Volkova et al. 2000, Chin et al. 2001), sometimes followed by saturation (Volkova et al. 2000, Fujita et al. 1999).

The three sets of ferrofluid-based samples investigated in this work have different values of the volume fraction of magnetic nanoparticles and of the micron-sized Fe particles, summing up the total particle volume fraction. The dynamic (Bingham) yield stress  $\tau_B$  increases for all the values of the total particle volume fraction and of the magnetic induction. The F 1000 set having the greatest nanoparticle volume fraction is an exception, evidencing the role of composition. Saturation of the increase of  $\tau_B$  is observed for  $B > 400$  mT at  $\Phi_{Fe} = (20 \div 25)\%$ . The same behavior of the static yield stress  $\tau_y$  is observed for this set having the most concentrated FF carrier. In case of the samples of the F 100 and F 500 sets, the static yield stress  $\tau_y$  shows saturation for  $\Phi_{Fe} = (20 \div 25)\%$ , for practically all values of the magnetic induction  $B$ .

Related to the explored wide range of the total volume fraction of particles, it is worth to evidence the role of the steric stabilizing layer coating the individual magnetic nanoparticles of the ferrofluid carrier. The chemisorbed oleic acid monolayer determines the hydrodynamic size and the hydrodynamic volume fraction of nanoparticles  $\varphi_h$ , which are much greater than the solid size (without coating) and the solid volume fraction  $\varphi$ , respectively. The ratio between the hydrodynamic

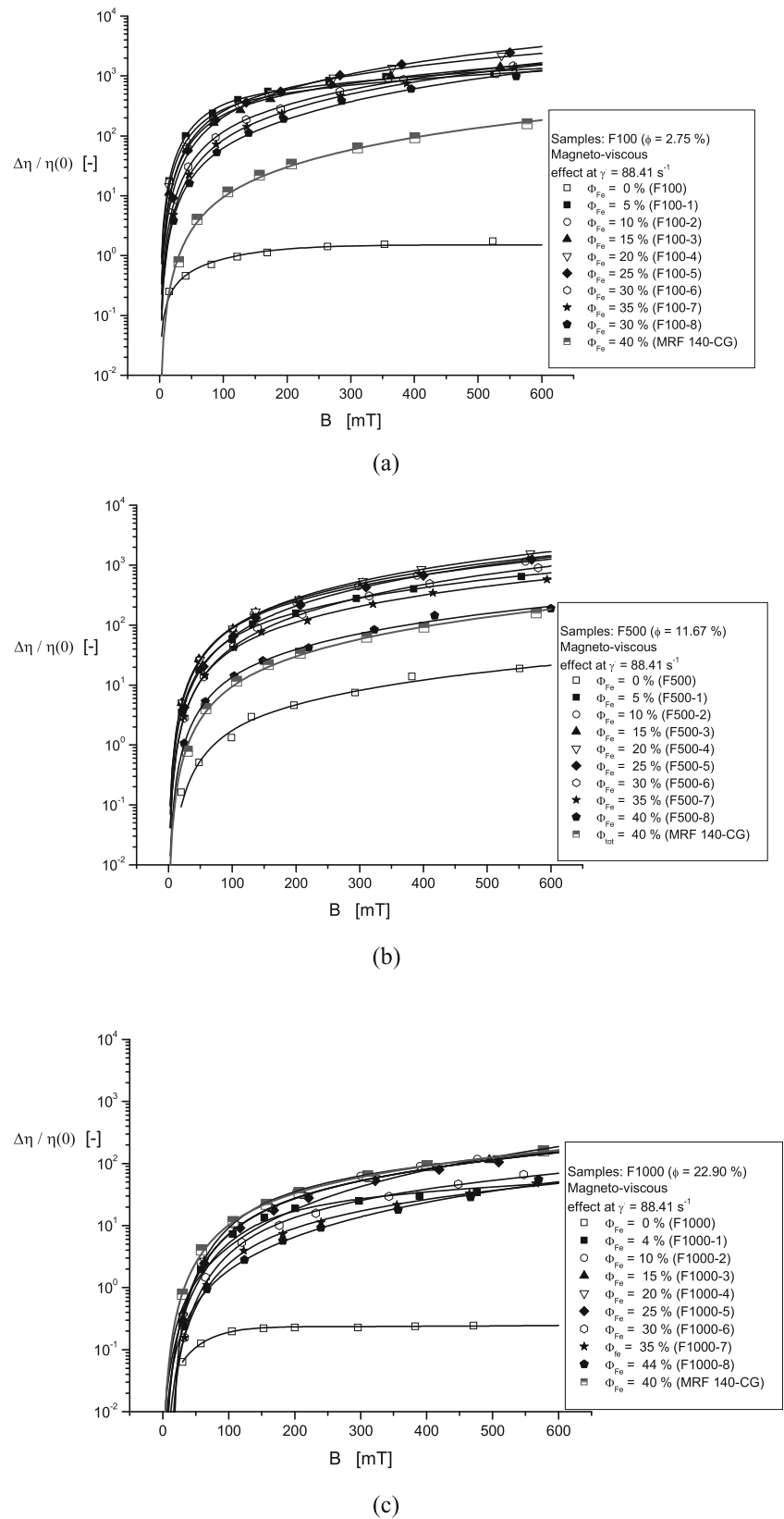
**Fig. 10** The magnetoviscous effect for shear rate  $\dot{\gamma} = 7.85 \text{ s}^{-1}$ ; fits for the commercial sample MRF 140 CG and for the three sets of samples: **a** F 100, **b** F 500, and **c** F 1000



volume fraction  $\phi_h$  and the solid volume fraction  $\phi$  was found from viscosity measurements to be 2.825 at

25 °C (Susan-Resiga et al. 2012) for the same type of ferrofluid as that used in this work. Consequently, the

**Fig. 11** The magnetoviscous effect for shear rate  $\gamma = 88.41 \text{ s}^{-1}$ ; fits for the commercial sample MRF 140 CG and for the three sets of samples: **a** F 100, **b** F 500, and **c** F 1000



hydrodynamic volume fraction of the most concentrated ferrofluid carrier F 1000 is  $\varphi_h \approx 0.65$ . Inserting this

value instead of the solid volume fraction  $\varphi$  into the formula  $\Phi_{tot} = \Phi_{Fe}(1 - \phi) + \phi$ , together with the highest

Fe volume fraction  $\Phi_{Fe} = 0.44$ , we find the upper limit of the effective total volume fraction of approximately 0.85 for the samples considered in this work. Taking into account the extremely bidisperse character of the suspensions, i.e., the ratio between the mean sizes of large and small particles of 0.001 and the elastic nature of the organic coating of nanoparticles, the achieved overall packing fraction is quite reasonable (Farr and Groot, 2009).

### Magnetoviscous effect

The relative increase of the viscosity  $\left(\frac{\Delta\eta}{\eta(0)} = \frac{\eta(B) - \eta(0)}{\eta(0)}\right)$  induced by the magnetic field, for two values of the shear rate,  $\gamma = 7.85 \text{ s}^{-1}$  and  $\gamma = 88.41 \text{ s}^{-1}$ , is represented in Figs. 10 and 11, for the three sets of FF-based MR fluids and for the commercial sample (MRF 140 CG). The fits were performed in a

similar way as for the yield stress, applying the same procedure and using formula (3):

$$\frac{\Delta\eta}{\eta(0)} = \frac{\eta(B) - \eta(0)}{\eta(0)} = c_1 \left(\frac{B}{B^*}\right)^2 \left[1 - \tanh\left(\frac{B}{B^*}\right)\right] + c_2 \Phi_{tot}^n \left(\frac{B}{B^*}\right)^m \tanh\left(\frac{B}{B^*}\right) \quad (3)$$

As expected, the magnetoviscous effect is the most reduced for the set F 1000, because these samples have the highest viscosities in the absence of the field.

The values of the parameters  $c_1$ ,  $c_2$ ,  $n$ , and  $m$  resulted by fitting  $\frac{\Delta\eta}{\eta(0)} = f(B)$  to the data outlined in Figs. 10 and 11 do not show a monotonic variation, as it was the case of the yield stresses  $\tau_B = \tau_B(B)$  and  $\tau_y = \tau_y(B)$ , because the relative viscosity does not increase monotonically with the particle volume fraction. The fit parameters were found to vary in the following intervals:

- 
- For  $\gamma = 7.85 \text{ s}^{-1}$ :  $c_1 = (0.13 \div 2652.92) \text{ Pa}$ ;  $c_2 = (6.88 \div 1713.88) \text{ Pa}$ ;  $m = (0.06 \div 1.94)$ ;  $n = (2.36 \div -0.004)$
  - For  $\gamma = 88.41 \text{ s}^{-1}$ :  $c_1 = (0.13 \div 356.8) \text{ Pa}$ ;  $c_2 = (7.19 \div 322.68) \text{ Pa}$ ;  $m = (0.0004 \div 2.49)$ ;  $n = (3.00 \div 0.0001)$
- 

### The influence of particle volume fraction on the magnetoviscous effect

The dependence of the magnetoviscous effect on the particle volume fraction at different values of the magnetic induction for the investigated samples is illustrated in Figs. 12 and 13 for all sets of samples.

The magnetoviscous effect, as it follows from Figs. 12 and 13, increases for greater magnetic induction values, however, in a different way as that observed for the MR effect. It is more intense for the sets F 100 and F 500 than for F 1000 due to the much higher viscosity of samples of this set in the absence of the applied magnetic field. The relative viscosity change shows an abrupt increase for the first sample of each set (F 100–1, F 500–1, F 1000–1), followed by a moderate increase up to  $\Phi_{Fe} = (20 \div 25)\%$  iron particle content. As it may be seen, the magnetoviscous effect does not increase continuously with the added Fe particles; therefore, the fit parameters resulted for the fitted curves in Figs. 10 and 11 obtained using formula (3) do not have a regular increase or decrease with the particle volume fraction or the magnetic induction. For example, the magnetoviscous effect is more pronounced for the sets F 100 and F 500 in comparison with that measured for the commercial sample. In case of samples of the set F 1000 for Fe content

greater than  $\Phi_{Fe} = (30 \div 35)\%$ , the magnetoviscous effect is smaller than that corresponding to MRF 140 CG.

### Conclusions

Twenty-seven ferrofluid-based magnetorheological fluid samples were formulated which cover a wide range of the magnetic particles solid volume fraction values at the two hierarchical levels involved, from 2.75 to 22.90 % (sub-domain magnetite nanoparticles) at the nanometer level and from 0 to 44 % (multi-domain iron particles) at the micrometer level, involving a size ratio of 1000 of the large to small size particles. The maximum solid particle volume fraction achieved of 56.82 % corresponds actually to an effective total particle volume fraction of 85 %. This includes the contribution of the chemisorbed organic layer coating of individual magnetic nanoparticles increasing their mean diameter with a factor of 2.825, which is the hydrodynamic size relevant for the magnetorheological behavior of the composite fluid samples. As the hydrodynamic volume fraction of magnetite nanoparticles attains 65 %, the upper limit for random packing, the composition of samples investigated covers practically the whole possible ranges both for nanometer- and micrometer-

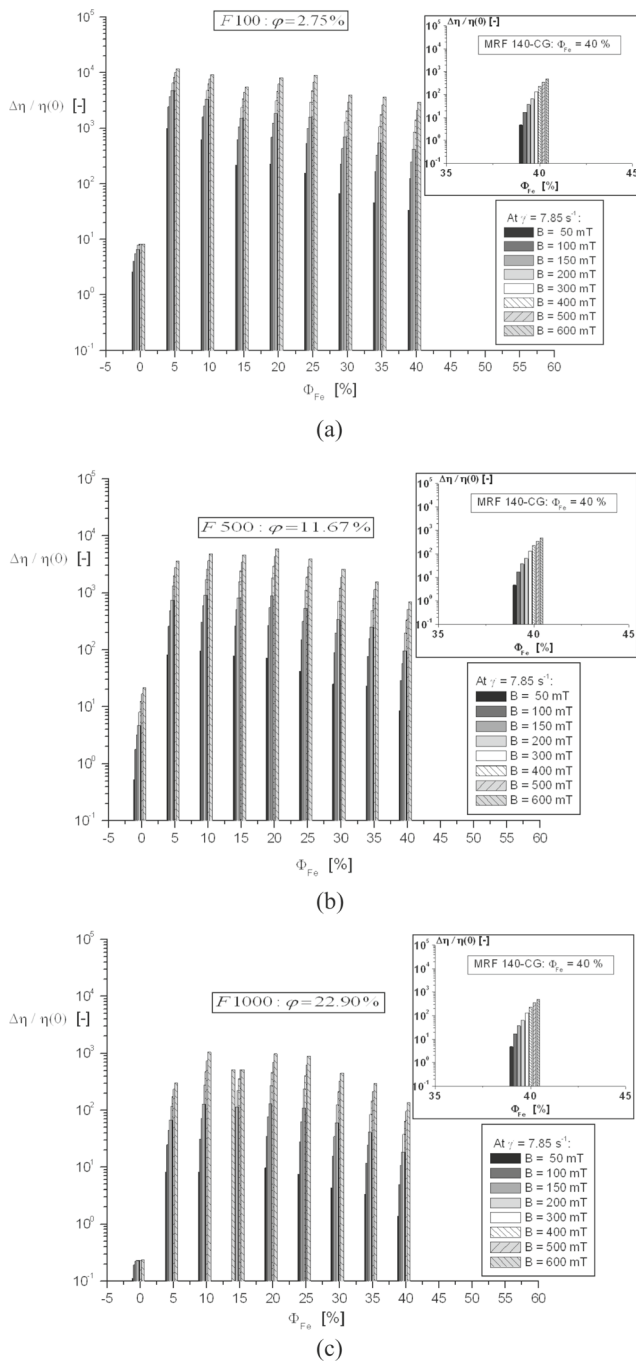


**Fig. 12** The dependence of the relative increase of viscosity  $\frac{\Delta\eta}{\eta(0)} = f(\Phi_{tot})$  for different values of the magnetic induction  $B$ , at shear rate  $\gamma = 7.85 \text{ s}^{-1}$ —commercial sample MRF 140 CG and: **a** set F 100, **b** set F 500, and **c** set F 1000

size magnetic particles. Thorough reproducibility tests performed proved the absence of any wall slip effects influencing the measurements. The Bingham and static yield stresses increase with both the magnetite NP volume fraction and the Fe particle volume fraction and, consequently, with the total particle volume fraction. The MR effect is more intense for the ferrofluid-based MR fluids than for the commercial MRF,

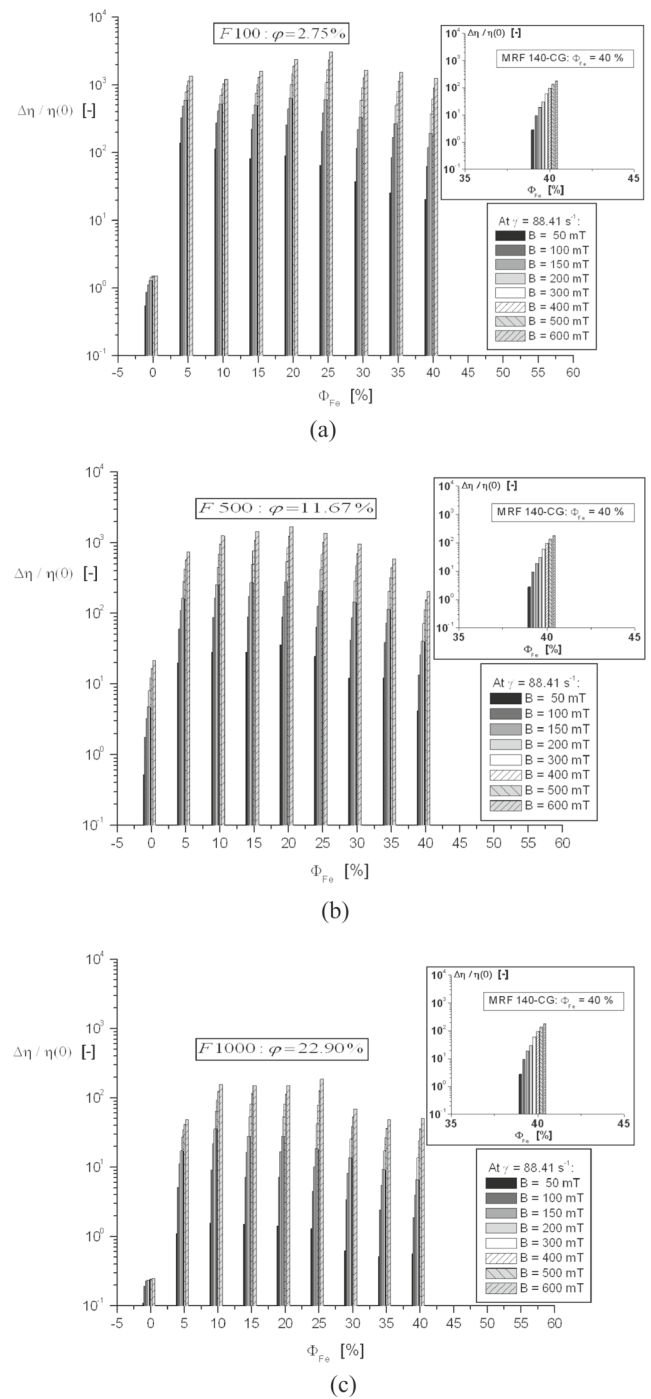


**Fig. 13** The dependence of the relative increase of viscosity  $\frac{\Delta\eta}{\eta(0)} = f(\Phi_{tot})$  for different values of the magnetic induction  $B$ , at shear rate  $\gamma = 88.41 \text{ s}^{-1}$ —commercial sample MRF 140 CG and: **a** set F 100, **b** set F 500, and **c** set F 1000

evidenced in the diagrams illustrating the dependence of the yield stresses (static and dynamic) on the volume fractions of nanometer- and micrometer-size particles ( $\phi$  and  $\Phi_{Fe}$ ). The magnetoviscous effect is more pronounced for the sets F 100 and F 500 in comparison with that measured for the commercial MR fluid.

The wide range of magnetorheological data correlated with nanolevel and microlevel composition details provide adequate choice of the composition required by various kinds of devices using ferrofluid-based MRFs. To exemplify, for high-pressure rotating seals, the F 1000 set is envisaged; already for 5 % Fe content, the saturation magnetization is twice higher providing the same increase of the sealing capacity, while keeping the magnetoviscous effect at an acceptable level for long-term exploitation. The choice for MR brakes designed for hydraulic runners is quite different and goes to set F 500, to a sample with high Fe content, approximately 30 %, to ensure relatively low off-state viscosity and high field induced yield stress. The sedimentation–redispersion issue is to be considered for any MR device. The redispersion of F 100 samples and of the MRF 140 CG sample proved to be more difficult than in case of the F 500 and F 1000 sets with higher concentration of magnetite nanoparticles; therefore, the samples with higher nanoparticle content are recommendable.

**Acknowledgments** This work was supported by the SEMNAL MRD research project (contract nr. 77/2014-PNII-UEFISCDI) and by the Research Program LLM-CCTFA 2013-2015 of the Romanian Academy. The ferrofluid carriers and the nano–micro composite MR fluid samples were prepared by Florica Balanean, Research Ass. (RCESCF-University Politehnica Timisoara, Timisoara, Romania). The authors are indebted to Dr. Vlad Socoliuc (CFATR) for valuable discussions and to Dipl.-Phys. Oana Marinica, PhD fellow, for magnetization measurements and data interpretation concerning the most concentrated samples.

## References

- Barber DE (2013) *MR fluids at the extremes: high energy and low temperature performance of LORD MR fluids and devices*, Ch.4 in. RSC Smart Materials 6, Magnetorheology: Advances and Applications (Ed. N. Wereley) 74–95. doi:10.1039/9781849737548.
- Bica D, Potencz I, Vekas L, Giula G, Potra (Balanean) F (2000) Procedure to obtain magnetic fluids for seals. Rom Patent RO 115533:B1
- Borbath T, Bica D, Potencz I, Borbath I, Boros T, Vekas L (2011) Leakage-free rotating seal systems with magnetic nanofluids and magnetic composite fluids designed for various applications. *Int J Fluid Mach Syst* 4:67–75
- Borbath T, Borbath I, Günther S, Marinica O, Vékás L, Odenbach S (2014) Three-dimensional microstructural investigation of high magnetization nano–micro composite fluids using x-ray microcomputed tomography. *Smart Mater Struct* 23:055018
- Borin DY, Zubarev AY, Chirikov DN, Odenbach S (2014) Stress relaxation in a ferrofluid with clustered nanoparticles. *J Phys D Condens Matter* 26:406002
- Bosioc AI, Muntean S, Tanasa C, Susan-Resiga R, Vékás L (2014) Unsteady pressure measurements of decelerated swirling flow in a discharge cone at lower runner speeds. *IOP Conference Series Earth Environ Sci* 22:032008. doi:10.1088/1755-1315/22/3/032008
- Bossis G, Volkova O, Laci S and Meunier A (2002) Magnetorheology: fluids, structures and rheology, in: *Ferrofluids: Magnetically Controllable Fluids and their Applications*, Lecture Notes in Physics, ed Odenbach S., 594:202–230
- Cabuil V, Bacri JC, Perzynski R, Yu R (1996) Colloidal stability of magnetic fluids. In: Berkovski B, Bashtovoy V (eds) *Magnetic fluids and applications handbook*. Begell House Inc., New York, Wallingford, pp. 33–56
- Carlson JD, Jolly MR (2000) MR fluid, foam and elastomer devices. *Mechatronics* 10(4–5):555–569. doi:10.1016/S0957-4158(99)00064-1
- Chin BD, Park JH, Kwon MH, Park OO (2001) Rheological properties and dispersion stability of magnetorheological (MR) suspensions. *Rheol Acta* 40:211–219
- Durairaj R, Man LW, Ekere NN, Mallik S (2010) The effect of wall-slip formation on the rheological behaviour of lead-free solder pastes. *Mater Des* 31:1056–1062
- Farr RS, Groot RD (2009) Close packing density of polydisperse hard spheres. *J Chem Phys* 131:244104
- Friedman AJ and Dyke SJ (2013) Development and Experimental Validation of a New Control Strategy Considering Device Dynamics for Large Scale MR Dampers using Real Time Hybrid Simulation, Report IISL–003.
- Fujita T, Yoshimura K, Seki Y, Dodbiba G, Miyazaki T, Numakura S (1999) Characterization of magnetorheological suspensions for seal. *J Intel Mater Syst Struct* 10:770–774
- Ginder JM, Davis LC, Elie LD (1996) Rheology of magnetorheological fluids: models and measurements. *Int J Mod Phys B* 10:3293–3303
- Iglesias GR, López-López MT, Durán JDG, González-Caballero F, Delgado AV (2012) Dynamic characterization of extremely bidisperse magnetorheological fluids. *J Colloid Interface Sci* 377: 153–159
- Iglesias GR, Ahualli S, Echávarri Otero J, Fernández Ruiz-Morón L, Durán JDG (2014) Theoretical and experimental evaluation of the flow behavior of a magnetorheological damper using an extremely bimodal magnetic fluid. *Smart Mater Struct* 23:085028(11pp)
- Iglesias GR, Fernández Ruiz-Morón L, Durán JDG, Delgado AV (2015) Dynamic and wear study of an extremely bidisperse magnetorheological fluid. *Smart Mater Struct* 24:127001
- Klingenberg DJ (2001) Magnetorheology: applications and challenges. *AICHE J* 47(2):246–249
- Klingenberg DJ, Ulicny JC, Golden MA (2007) Mason numbers for magnetorheology. *J Rheol* 51(5):883–893
- Laun HM, Schmidt G, Gabriel C, Kieburg C (2008) Reliable plate–plate MRF magnetorheometry based on validated radial magnetic flux density profile simulations. *Rheol Acta* 47(9):1049–1059
- Laun HM, Gabriel C, Kieburg C (2010) Twin gap magnetorheometer using ferromagnetic steel plates—performance and validation. *J Rheol* 54(2):327
- Liu YD, Choi HJ (2012) Carbon nanotube-coated silicated soft magnetic carbonyl iron microspheres and their magnetorheology. *J Appl Phys* 111:07B502
- Liu YD, Hong CH, Choi HJ (2012) Polymeric colloidal magnetic composite microspheres and their magneto-responsive characteristics. *Macromol Res* 20(12):1211–1218
- López-López MT, de Vicente J, Bossis G, González-Caballero F, Durán JDG (2005) Preparation of stable magnetorheological fluids based on extremely bimodal iron–magnetite suspensions. *J Mater Res* 20(4):874–881
- López-López MT, Kuzhir P, Laci S, Bossis G, González-Caballero F, Durán JDG (2006) Magnetorheology for suspensions of solid particles dispersed in ferrofluids. *J Phys Condens Matter* 18:S2803–S2813
- Mezger TG (2002) *The Rheology Handbook*, Curt R. Vincentz Verlag, Hannover
- Ngatu GT, Wereley NM (2007) Viscometric and sedimentation characterization of bidisperse magnetorheological fluids. *IEEE Trans Magn* 43(6):2474–2476
- Park BJ, Fang FF, Choi HJ (2010) Magnetorheology: materials and application. *Soft Matter* 6:5246–5253

- Ramos J, Klingenberg DJ, Hidalgo-Álvarez R, de Vicente J (2011) Steady shear magnetorheology of inverse ferrofluids. *J Rheol* 55(1):127–152
- Rankin PJ, Horvath AT, Klingenberg DJ (1999) Magnetorheology in viscoplastic media. *Rheol Acta* 38:471–477
- Russell WB, Saville DA, Schowalter WR (1989) *Colloidal dispersions*, Cambridge Univ. Press, Cambridge
- Shah K, Phu Do X and Choi S-B (2014) Rheological properties of bi-dispersed magnetorheological fluids based on plate-like iron particles with application to a small-sized damper, *Journal of Applied Physics* 115:203907–203907-10. doi:10.1063/1.4879681
- Susan-Resiga D, Vékás L, Bica D (2010) Flow behaviour of extremely bidisperse magnetizable fluids. *J Magn Magn Mater* 322(20):3166–3172. doi:10.1016/j.jmmm.2010.05.055
- Susan-Resiga D, Socoliuc V, Boros T, Borbáth T, Marinica O, Han A, Vékás L (2012) The influence of particle clustering on the rheological properties of highly concentrated magnetic nanofluids. *J Colloids Interface Sci* 373:110–115
- Susan-Resiga D, Vékás L (2014) Yield stress and flow behavior of concentrated ferrofluid based magnetorheological fluids: the influence of composition. *Rheol Acta* 53:645–653
- Vékás L, Bica D, Avdeev MV (2007) Magnetic nanoparticles and concentrated magnetic nanofluids: Synthesis, properties and some Applications. *Particuology* 45:43–49
- Vékás L (2008) Ferrofluids and magnetorheological fluids. *Smart Mater Micro/Nanosyst Book Series Adv Sci Technol* 54:127–136. doi:10.4028/www.scientific.net/AST.54.127
- de Vicente J, Klingenberg DJ, Hidalgo-Álvarez R (2011) Magnetorheological fluids: a review. *Soft Matter* 7:3701–3710
- Viota JL, González-Caballero F, Durán JDG, Delgado AV (2007) Study of the colloidal stability of concentrated bimodal magnetic fluids. *J Colloid Interface Sci* 309:135–139
- Viota JL, Durán JDG, Delgado AV (2009) Study of the magnetorheology of aqueous suspensions of extremely bimodal magnetite particles. *Eur Phys J E* 29:87–94
- Volkova O, Bossis G, Guyot M, Bashtovoi V, Reks A (2000) Magnetorheology of magnetic holes compared to magnetic particles. *J Rheol* 44(1):91–104
- Wang X, Gordaninejad F (2006) Study of magnetorheological fluids at high shear rates. *Rheol Acta* 45:899–908
- Wereley NM, Chaudhuri A, Yoo J-H, John S, Kotha S, Suggs A, Radhakrishnan R, Love BJ, Sudarshan TS (2006) Bidisperse magnetorheological fluids using Fe particles at nanometer and micron scale. *J Intell Mater Syst Struct* 17:393–401. doi:10.1177/1045389X06056953
- Yang Y, Li L, Chen G (2009) Static yield stress of ferrofluid-based magnetorheological fluids. *Rheol Acta* 48:457–466
- Yoshimura A, Prud'homme RK (1988) Wall-slip corrections for coquette and parallel disk viscometer. *J Rheol* 32:53–67
- Zhou JZQ, Fang T, Luo G, Uhlherr PHT (1995) Yield stress and maximum packing fraction of concentrated suspensions. *Rheol Acta* 34:544–561
- Zhu X, Jing X, Cheng L (2012) Magnetorheological fluid dampers: a review on structure design and analysis. *J Intell Mater Syst Struct* 23(8):839–873. doi:10.1177/1045389X12436735